IEEE Access
Multidisciplinary | Rapid Review | Open Access Journal

Received 20 June 2023, accepted 16 July 2023, date of publication 21 July 2023, date of current version 31 July 2023.

Digital Object Identifier 10.1109/ACCESS.2023.3297878

RESEARCH ARTICLE

Design and Analysis of Patch Antenna With 244° 3-dB Axial Ratio Beamwidth

BO-WEN ZHENG, BO YUAN, PENG ZHAO, (Member, IEEE), AND GAO-FENG WANG, (Senior Member, IEEE)

MOE Engineering Research Center of Smart Microsensors and Microsystems, School of Electronics and Information, Hangzhou Dianzi University, Hangzhou 310018, China

Corresponding author: Bo Yuan (yuanbo@hdu.edu.cn)

This work was supported in part by the National Natural Science Foundation of China under Grant 62141409, and in part by the Zhejiang Provincial Key Research and Development Fund under Grant 2021C01041.

ABSTRACT A novel design approach for broadening 3-dB axial ratio beamwidth (ARBW) of circular polarization (CP) patch antenna is herein introduced. A patch structure consisting of three pairs of slots and four coupled strips is firstly proposed and examined. In such a compact size of 0.216 $\lambda_0 \times 0.216\ \lambda_0 \times 0.013\ \lambda_0$ (λ_0 is the free-space wavelength at the 2.42 GHz). By carefully studying the evolution and related impact of the patch structure, the ARBW broadening mechanism is thoroughly revealed. The far-zone fields are further studied by the theory of equivalent magnetic currents (EMCs), and two polarized degenerate modes TM10 and TM01 are generated to excite CP radiation. To better understand the working mechanism of the proposed parasitic structures, an equivalent circuit consisting of three networks is given. Finally, to validate the performance, the proposed antenna is fabricated and measured, the simulated and measured results of impedance bandwidth for $|S_{11}| \leq -10$ dB is from 2.36 GHz to 2.48 GHz, and the measured 3-dB ARBW is 244° at plane $\varphi = 0°$. Both simulated and measured results show that the proposed antenna is very promising for high elevation angle wireless applications.

INDEX TERMS 3-dB axial ratio beamwidth (ARBW), circular polarization (CP), coupled strips, compact size, equivalent magnetic currents (EMCs), degenerate modes.

I. INTRODUCTION

Circularly polarized (CP) antennas play an important role in many wireless applications, such as the radio frequency identification (RFID), global positioning systems (GPS), and wireless power transmission systems. Because the CP antennas do not require strict alignment between transmitting and receiving antennas, they can also combat the multipath fading and are immune to the 'Faraday rotation' effect due to ionosphere [1]. In addition, microstrip patch antennas (MPAs) [2] own unique characteristics: low profile, small size, light weight, easy to fabricate, etc.. Therefore, MPAs with CP characteristic would be a good candidate for the application scenarios that require low-cost, easiness to mount, and high robustness to polarization mismatch [3].

The associate editor coordinating the review of this manuscript and approving it for publication was Hussein Attia.

For CP antenna with high beam, it is valuable for GNSS applications [4], such as navigation, positioning, public safety/surveillance, geographic surveys, time standards, mapping, weather, and atmospheric information. Under this background, a low-profile circularly polarized microstrip antenna is exceedingly demanded. However, the traditional CP antennas suffer from a relatively narrow 3-dB ARBW [5].

Several methods were introduced to widen the 3-dB ARBW in the past two decades. Those methods can be classified into four typical approaches. The first approach was implemented by utilizing three-dimensional stacked structures, such as tapered elliptical cavity [6] and other reflector structures [7]. The 3-dB ARBWs were mainly affected by the reflected waves from the metallic wall of the cavity or reflector surface.

The second way was employing distinct dipoles to adjust electrical current component to better achieve CP radiation. In [8], a CP antenna with two pairs of folded dipoles in

a square contour was reported. The antenna had the 3-dB ARBW at the central frequency of 1.6 GHz, and the 3-dB ARBW was extended to 135° at $\varphi = 0°$ and 142° at $\varphi = 90°$, respectively. In addition, the crossed-dipole CP antenna was proposed in [9] and [10], and the 3-dB ARBW was more than 120°.

The third method was realized by adding special metasurface structure or high-permittivity substrate to reduce dielectric loss and improve the CP radiation performance. In addition, the μ-negative transmission lines with metamaterials were used in [11], and the 3-dB ARBW varied from 175° to 190°.

Finally, the fourth approach was realized by introducing additional parasitic structures to change the flow-path of surface current to excite CP radiation. Such additional parasitic structures include rectangular slots [12], [13], rectangular strips [14], [15], unequal circular-patches [4], integrated asymmetric/symmetric-stubs [16] and metallic vias [17]. Two-pair of parallel slots were orthogonally etched on a circular patch antenna [18], which was operated at LHCP radiation with wide 3-dB ARBW of 228° and 214° at $\varphi = 0°$ and $\varphi = 90°$, respectively.

A novel CP patch antenna with wide 3-dB ARBW is herein introduced. It offers wide 3-dB ARBW. The polarized degenerate modes TM_{10} and TM_{01} are used to excite the CP radiation. This antenna operates in right-handed circular polarization (RHCP) at broadside radiation. The equivalent circuit, which is in good agreement with the full-wave electromagnetic simulation, is constructed for this antenna. Section II illustrates the geometry and operating principles of the proposed CP antenna. The simulated and measured results of the proposed CP antenna are shown in Sections III. Finally, conclusions are given in Section IV.

II. CIRCULAR POLARIZATION PATCH ANTENNA

The geometry of the proposed CP patch antenna is illustrated in Fig. 1. Its dielectric substrate FR4 has relative permittivity of $\varepsilon_r = 4.4$, loss tangent of 0.02 and thickness of 1.575 mm. The ground plane and radiating patch, which mainly serve to achieve directional radiation, are printed on the bottom and top surface of substrate, respectively. Its overall size is 60×60 mm^2 and fed by a 50-Ω coaxial feed. In addition, the radiation patch is symmetric about its center and consists of three pairs of 45° rotated slots and four strips with shorted metallic vias closely coupled to the patch. Table 1 lists the detailed antenna parameters.

A. ANTENNA EVOLUTION

Fig. 2 is the structural evolution process of the proposed antenna. The four antennas are named as antenna 1 (Ant 1), antenna 2 (Ant 2), antenna 3 (Ant 3), and antenna 4 (Ant 4), respectively. From the operating principle of typical diagonal slot antennas [19], the narrow diagonal slot can be equivalent to an ideal magnetic wall, which can control the surface current of the patch to excite two polarization degenerate modes

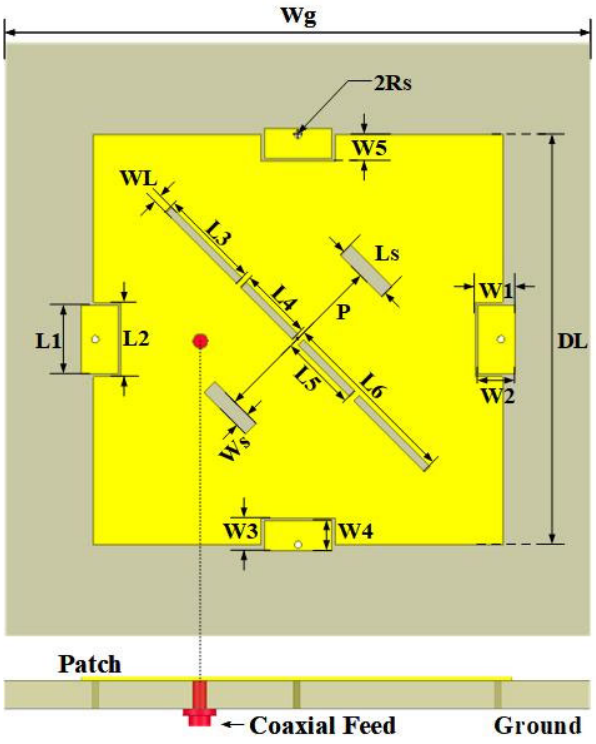

FIGURE 1. Geometry of the proposed antenna.

TABLE 1. Parameters of the CP antenna (mm).

DL	P	L1	L2	L3	L4
27	12	4.2	5	6.5	4.9
L5	L6	Rs	Ws	W1	W2
5	6	0.25	1.5	2.6	2.4
W3	W4	W5	Ls	WL	Wg
2.1	2	1.4	4	0.51	60

with phase difference of 90°, so CP radiation can be realized. Ant 1 is evolved from a typical slot MPA, in which a narrow slot with 45° inclination is etched inside a square patch [13]. Ant 1 can generate two electric field components that differ 90° in phase and are equal in amplitude over a certain angular range. Similar to Ant 1, a pair of slots with 45° inclination is etched inside a square patch [12]. In general, the slot length in Ant 2 is different from that in Ant 1. In Ant 3, two pairs of additional symmetrical inclined slots are etched around the aforementioned slots in Ant 2 and all of the slots are parallel and symmetric about the center of the patch. At last, Ant 4 is the final form of the evolution antenna, in which four coupled strips with metallic vias are inserted around the patch from Ant 3. In these four antennas, all the slots have the same width, and all the radiation patches (except Ant 4) have the same size. In the following, the improvements of antenna

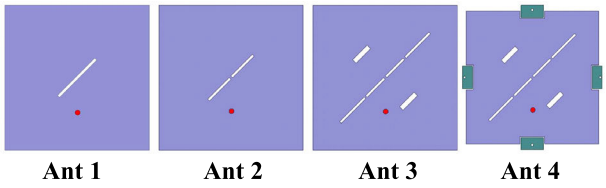

FIGURE 2. Evolution of the CP antenna from antenna 1 to 4.

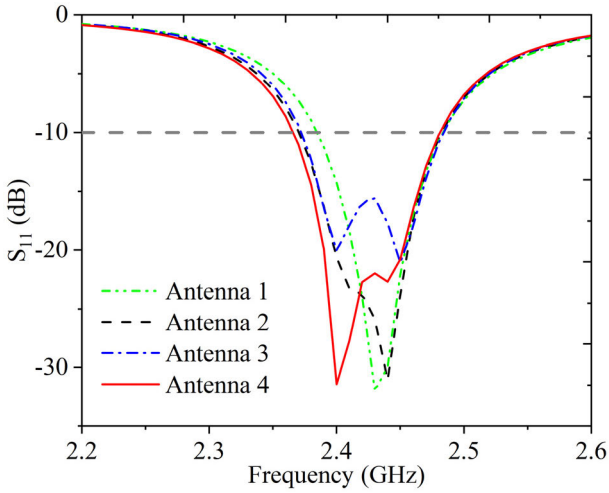

FIGURE 3. Simulated results of $|S_{11}|$ for antennas 1-4.

characteristics due to the added structures will be examined. In order to make meaningful performance comparisons, the lengths of slots are used for tuning these four antennas to operate at the same frequency, i.e., 2.42 GHz. Hence, the performance of each individual antenna may not be optimal.

The simulation results of $|S_{11}|$ and axial ratio (AR) for the above four antennas are shown in Fig. 3 and Fig. 4, respectively. The simulation results are obtained by using a full-wave electromagnetic simulator (e.g., HFSS). From Fig. 3 and Fig. 4, the impedance bandwidth (IBW) of Ant 1 is the narrowest with one resonant frequency, and its 3-dB ARBW is exceedingly narrow, which is only 72°. In Ant 2, by adding an extra slot, the IBW is improved and the 3-dB ARBW is around 110° of θ. For Ant 3, the CP performance also depends on the orthogonal electric field component excited by the slots. Comparing to the Ant 1 and Ant 2, the extra slots can optimize amplitude difference and phase difference of two electric field components in a wider range angle, and the 3-dB ARBW is widen as 209° from −103° to 106° with CP radiation.

Finally, it can be observed that the IBW of Ant 4 is near 120 MHz, which is the largest one among the four antennas. In Ant 4, the gaps between the two pairs of strips and the radiation patch result in parasitic capacitances, whereas the metallized vias can introduce parasitic inductances. Equivalently, an extra LC resonant circuit is added, which can expand the impedance bandwidth. The reactance introduced in the x-axis and y-axis can increase the electric length of the

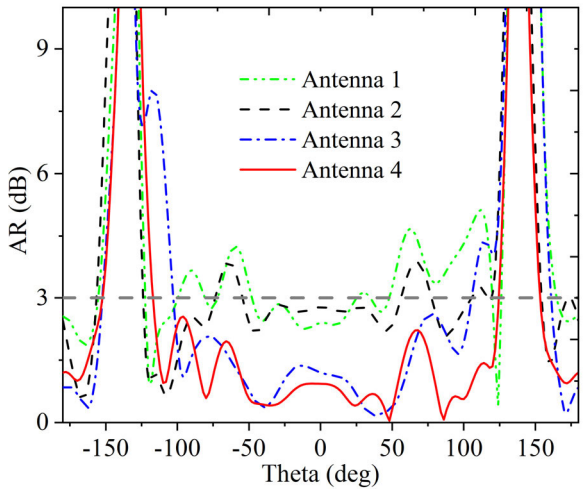

FIGURE 4. Simulated results of AR beamwidth for antennas 1-4.

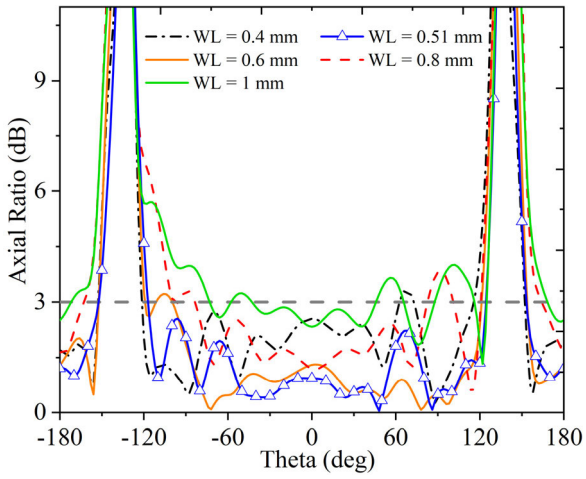

FIGURE 5. Simulated AR of the proposed antenna with different WL.

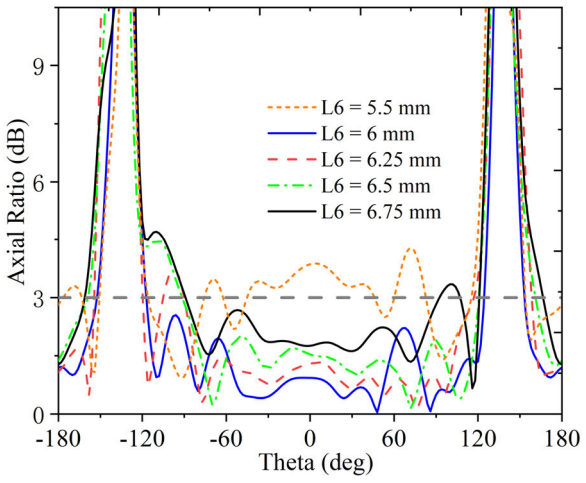

FIGURE 6. Simulated AR of the proposed antenna with different L6.

corresponding axis, and thus reduce the proposed antenna. In addition, its 3-dB ARBW can reach to 241°. That is, the CP radiation coverage of wide angle can be realized in Ant 4. The reason for the wide ARBW is that the shorted pins

provide vertical polarization whereas the slots can generate horizontal polarization with capability of better adjusting CP performance [20]. By the way, the CP performance will be deteriorated with the number of metal biases decreased, because the phase and amplitude differences of electric field components are deviated 90° and 0 dB, respectively. Moreover, the three pair of narrow slots are placed to serve as magnetic dipoles with quarter wavelength separation, forcing the amplitude of the orthogonal electric field components to be equal across a wide angle [12].

The 3-dB ARBW of the CP antenna is a strong function of the mutual magnetic field, which can be tuned with the slot parameters. To understand influences of the slot parameters (i.e., slot width, slot length and so on), a set of studies on the slot parameters is carried out while keeping the dimensions and location of the strips and metallic vias unchanged. In Fig. 5, the ARBW can achieve the optimum performance when WL = 0.51 mm, in which a wide ARBW about 241° is obtained. The effect of different L6 on AR is shown in Fig. 6, with respect to its optimized value of 241° at L6 = 6 mm. In principle, the subtle adjustment of a slot size can affect the characteristics of the magnetic dipole generated by the corresponding slot and changes the current distribution and intensity around the slot, which affect the amplitude and phase of the orthogonal electric components, resulting in a change on ARBW. With increasing L6, the ARBW becomes narrower. Specifically, the beamwidth turns to be sharply reduced when the effective patch width exceeds the critical value. Therefore, by properly adjusting the slot parameters, a better AR performance can be achieved in the proposed antenna.

B. TM MODEL ANALYSIS

According to the radiation principle of CP antenna, when the phase and amplitude differences of electric field components are near 90° and around 0 dB, respectively, two polarized degenerate modes of TM_{10} and TM_{01} can be generated to excite CP radiation. Since the thickness of the proposed single-fed MPA is much smaller than λ_g(where λ_g is the guided wavelength at 2.42 GHz), the electric field of the antenna can be analyzed by virtue of cavity model theorem [21], and its far-zone radiated fields can be theoretically studied by using equivalent magnetic currents (EMCs) [19].

In Fig. 7 (a), the electric field distribution and equivalent magnetic currents (EMCs) of the antenna under operation are presented. It can be seen that the electric field, which is normal to the patch, changes alternately in one half of the wavelength travelling on the side of the patch along the x-axis. In the y-axis, the direction of electric field remains unchanged. Thus, one can conclude that the antenna operates in TM_{10} mode. Also, it can be seen that its electric field changes once along the x-axis, resulting in reverse EMCs along the x-axis (marked in the green color), and the EMCs are offset due to the opposite direction along the x-axis. From the perspective of the surface current and based on the right-hand rule, the magnetic field in the substrate is continuous, so almost no current passes through the metallic vias. In contrast, the electric field of EMCs along the y-axis (marked in the red color) has no transverse phase reversal, and the parallel EMCs along the y-axis are in the same direction.

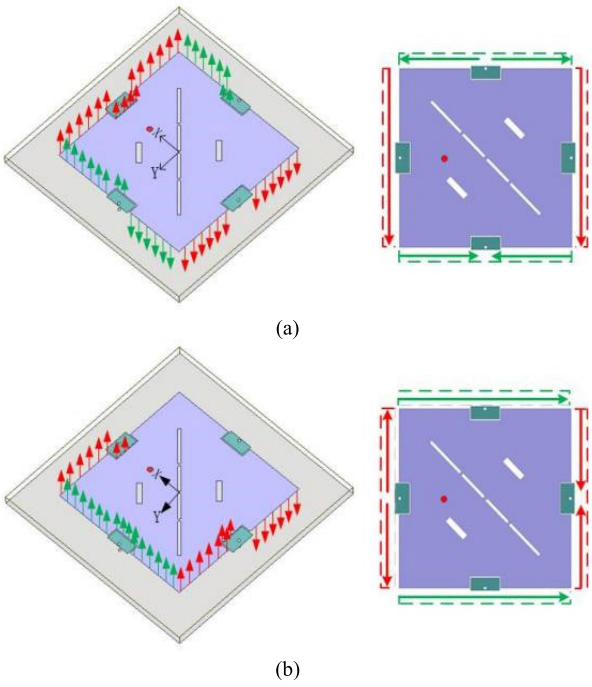

FIGURE 7. Electric field distributions underneath the radiating patch of the proposed CP antenna. (a) TM10 at 2.4 GHz, and (b) TM01 at 2.44 GHz.

Similarly, the TM_{01} mode and corresponding EMCs are shown in Fig. 7 (b). According to the above results, one can draw a conclusion that the broadside radiation mainly owes to the alternatively EMCs along the y-axis in Fig. 7 (a). On the other hand, the EMCs along the x-axis mainly contributes to the CP radiation in Fig. 7 (b).

To further investigate the CP resonant mode of the structure, the simulated current and magnetic field distributions on the patch at 2.42 GHz is plotted in Fig. 8, where T denotes the period. It can be observed that the current distribution is time-dependent and rotating, and the dominant surface current is along the y-axis at t = 0 and corresponding to the conventional TM_{01} mode, as shown in Fig. 7 (b). In addition, the structure is symmetric and the surface current is mainly concentrated around the slots. The directions of electric current at t = T/4, t = T/2, and t = 3T/4 are all kept along the positive x-, negative y-, and negative x-axes, respectively. By changing the time, the current direction rotates in the counterclockwise direction, so it exhibits right-handed circular polarization (RHCP) radiation.

Moreover, a slot on a metallic patch serves as a magnetic dipole. It can be seen that the magnetic field at both ends of each slot is stronger than that in the middle of the slot. Due to the symmetry of its structure, the magnetic field distribution is perfectly symmetrical. The parasitic structures can generate

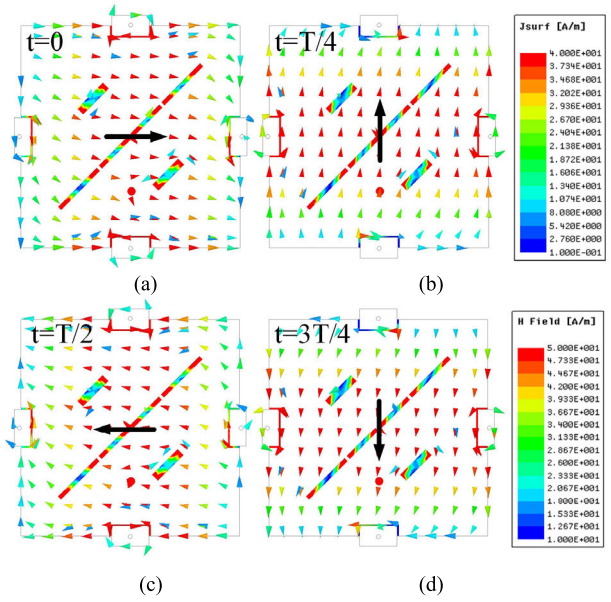

FIGURE 8. Simulated current and magnetic field distributions of the proposed CP antenna at 2.42 GHz. (a) t = 0, (b) t = T/4, (c) t = T/2, and (d) t = 3T/4.

two orthogonal electric field components, whereas the magnetic field mode of the radiation patch itself can be optimized to achieve CP performance over a wide angular range.

From [14], the ARBW is mainly determined by the phase differences between Eθ and Eφ rather than their amplitude ratios. In general, the axial ratio can be expressed as follows [22]:

$$\mathrm{AR} = \sqrt{\frac{1+\rho^2+\sqrt{\rho^4+2\rho^2\cos(2\Delta\phi)+1}}{1+\rho^2-\sqrt{\rho^4+2\rho^2\cos(2\Delta\phi)+1}}} \quad (1)$$

where ρ is ratio of the electric field amplitudes of TM_{10} and TM_{01}, and ϕ represents the phase difference between the TM_{10} and TM_{01} signals. Then, the simulated results of phase difference and magnitude difference of |Eθ| and |Eφ| are shown in Fig. 9. It can be observed that the phase difference of Eθ and Eφ is near 90° (i.e., the dashed line), and the amplitude difference between Eθ and Eφ is close to 0 dB (i.e., the solid line) over a wide-angle range. Note that AR from (1) is dimensionless and shown in dB in Fig. 9. The above results indicate that a wide ARBW about 241° (i.e., from −117° to 124°) is obtained.

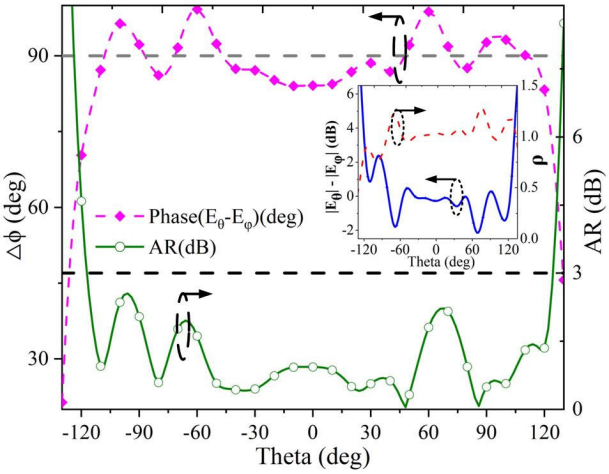

FIGURE 9. Simulated magnitude and phase of |Eθ| and |Eφ| components of the proposed CP antenna.

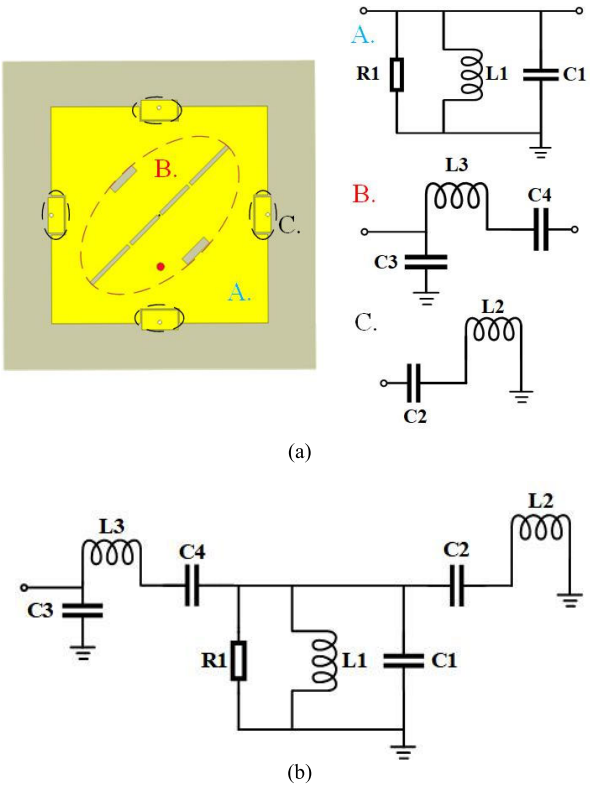

FIGURE 10. Equivalent circuit of proposed CP antenna. (a) three networks, and (b) complete circuit.

C. EQUIVALENT CIRCUIT

To better understand the working mechanism of the proposed parasitic structures, an equivalent circuit consisting of three networks A, B and C is given in Fig. 10 (a). In addition, the equivalent circuit model is constructed based on the inherent characteristics of antennas and the parasitic structure. Based on [22], the traditional MPAs without extra parasitic structure can be seen as a parallel circuit of RLC as Network A, which can excite a resonant frequency and generate a linearly polarized (LP) with TM_{01} mode [23]. Next, three pairs of 45° rotated slots and 50-Ω coaxial feed are modeled as Network B, in which C4 represents equivalent capacitor of the three pairs of diagonal slots, and C3 and L3 denote parasitic capacitor and inductor of the coaxial feed respectively. In principle, a slot within the metallic boundary behaves as a magnetic dipole [12]. Therefore, three pairs of slots at the center of the patch, which have 45° inclination with respect to the feeding axis, simultaneously excite two orthogonal modes by

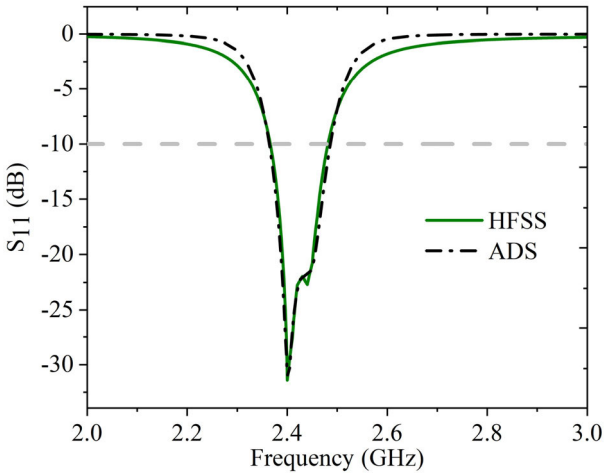

FIGURE 11. Comparison of $|S_{11}|$ between the proposed CP antenna and its equivalent circuit model in HFSS and ADS.

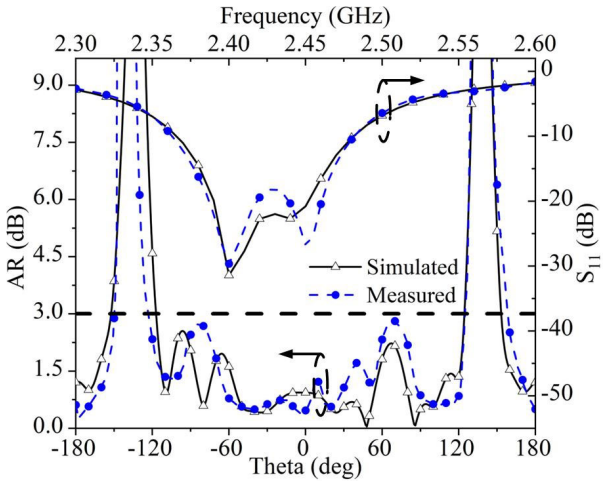

FIGURE 12. Simulated and measured $|S_{11}|$ and AR at plane $\varphi = 0°$ of the proposed CP antenna.

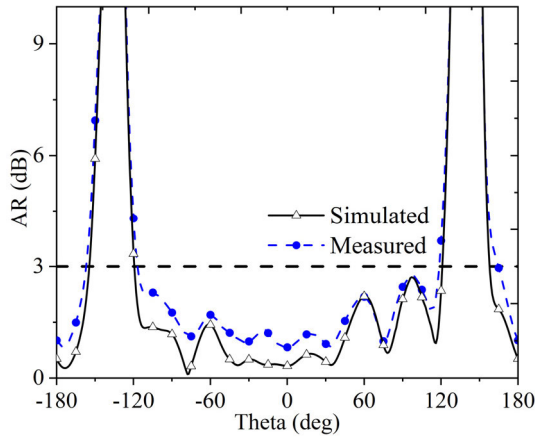

FIGURE 13. Simulated and measured AR at plane $\varphi = 90°$ of the proposed CP antenna.

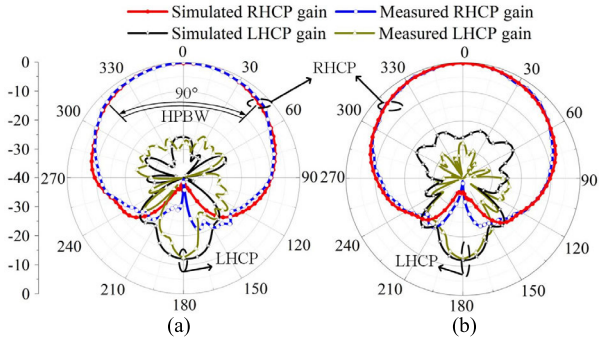

FIGURE 14. Simulated and measured LHCP and RHCP patterns at planes (a) $\varphi = 0°$ and (b) $\varphi = 90°$.

increasing the frequency of one mode without distracting the other that originates the CP radiation. In addition, the dimension and perturbation gap between the slots are manipulated to regulate the beamwidth of CP radiation.

Network C is an LC resonant circuit, which is aiming to widen the working bandwidth and optimize the amplitude and phase difference of two electric field components to achieve a wider CP radiation range. C2 and L2 are used to represent equivalent capacitor of the four narrow gaps and equivalent inductor of the four shorted metallic vias, respectively.

To further investigate the proposed antenna, the structure parameters have been extracted and studied. Also, the complete equivalent circuit is shown in Fig. 10 (b). The following is specific parameters: C1 = 1100 pF, C2 = 50 pF, C3 = 7 pF, C4 = 10.2 pF, R1 = 0.88 Ω, L1 = 3.7 pH, L2 = 100 nH, and L3 = 1 nH.

The simulated results of HFSS and Advance Design System (ADS) are shown in Fig. 11. It is obvious that the results are in a good agreement within the impedance bandwidth of −10 dB, which indicates that the equivalent circuit is a parametric expression of the antenna, and has intuitively modeled the antenna structure as a lumped circuit. Consequently, during the design process, modifying circuit topology parameters to adjust the parasitic is helpful in achieving circular polarization.

III. RESULTS AND DISCUSSION

The antenna is fabricated for testing. The simulated and measured results of AR and $|S_{11}|$ are shown in Fig. 12. In addition, $|S_{11}|$ of the proposed antenna is measured by using a Vector Network Analyzer, and the radiation pattern is obtained in the anechoic chamber. The simulated and measured results of impedance bandwidth for $|S_{11}| \leq -10$ dB is from 2.36 GHz to 2.48 GHz, the discrepancy is mainly caused by the fabrication errors in the location of the metallic vias and the size of etched slots. Moreover, the relative permittivity of the actually processed substrate also affects the impedance property. The simulated and measured results of 3-dB ARBW are 241° and 244° at plane $\varphi = 0°$, respectively. Also, the measured minimum AR is 0.4 dB. In addition, the simulated and measured results of 3-dB ARBW are 239° and 235° at plane $\varphi = 90°$ are shown in Fig. 13. Despite the antenna structure exhibiting mirror symmetry about the origin, the placement of the feed along the x-axis causes the current intensity to be non-completely symmetric, result in the AR

TABLE 2. Performance comparison between our proposed CP antenna and other previous works.

Antenna Tape	Antenna Size (λ^3)	IBW (%)	Substrate / Efficiency	CP Bandwidth (%)	HPBW	3-dB ARBW		XPD (dB)	
						$\Phi = 0°$	$\Phi = 90°$	$\Phi = 0°$	$\Phi = 90°$
unequal circular-patches [4]	0.373 × 0.373 × 0.016	3.47	Rogers 4003 / —	1.5	—	180	180	—	—
2 × 2 folded dipole array [8]	0.43 × 0.43 × 0.004	24	Rogers 4003 / 85%	5.6	84°	135°	142°	—	—
Vertical cross dipole with cavity [10]	0.57 × 0.57 × 0.296	46.3	Rogers 3006 / 82%	13	111°	211°	228°	30	30
				30.2	103°	202°	213°	20	20
Diagonal slot [12]	0.289 × 0.289 × 0.013	3.4	Rogers 5880 / —	0.93	—	226°	198°	17.7	15.3
Slots + Ring [13]	0.27 × 0.27 × 0.01	4.6	FR4 / —	1.02	—	160°	—	—	—
Coupled strips [14]	0.21 × 0.21 × 0.016	1.7	F4B / —	0.63	—	188°		—	—
Slotted [18]	π × 0.35 × 0.35 × 0.013	2.6	Rogers 5870 / —	0.9	92°	228°	214°	18	18
Pin_loaded [23]	0.41 × 0.41 × 0.02	2.71	F4B / —	0.65	—	140°	143°	—	—
The proposed CP antenna	0.216 × 0.216 × 0.013	5	FR4 / 60%	1.08	90°	244°	235°	27.7	27.7

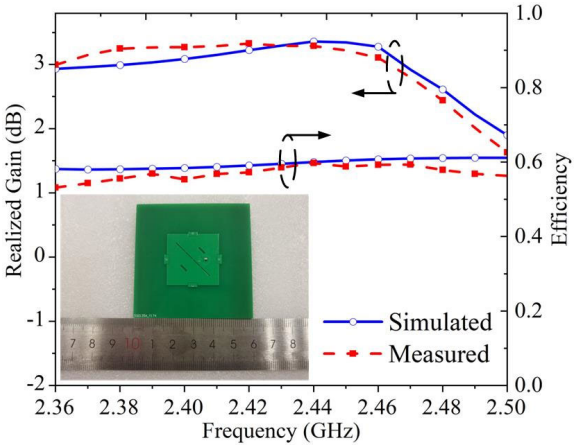

FIGURE 15. Simulated and measured results of gain and efficiency of the proposed CP antenna.

beamwidth patterns in Fig. 12 and 13 are not symmetrical wrt. theta axis. The simulated and measured radiation patterns for the two principal planes $\varphi = 0°$ and $\varphi = 90°$ are in the broadside direction, as shown in Fig. 14, in which a good agreement is observed between the simulated and measured results. It is obvious that the proposed antenna is operating in RHCP radiation. It is worth mentioning that the LHCP pattern has a larger back lobe while the RHCP has a better front-to-back ratio, because there is a finite ground [11], [24] and an antenna with a small ground plane inherently results in large back-radiation. For the proposed dual antenna, the size of ground plane can be increased to reduce the unfavorable back-radiation. However, the FBR and size of antenna have to be carefully compromised so that the antenna is miniaturized on the premise of ensuring the radiation performance. Also, the cross-polarization discriminations (XPD) are both 27.7 dB at planes $\varphi = 0°$ and $\varphi = 90°$, respectively.

The realized gains of the simulated and measured results are shown in Fig. 15, in which the inserted small figure shows actual photograph of the fabricated CP antenna. From Fig. 15, the measured realized gain varies from 3.12 dBic to 3.42 dBic and the efficiency is around 60% at the operational band. The dielectric substrate used in the antenna is FR4, which has a pitfall of high loss. In addition, to obtain higher efficiency, the dielectric substrate with lower loss angle tangent can be used to design the antenna. The performance comparison is tabulated in Table 2, the simulated HPBW is only 90°, by adjusting the embedded distance of the strips, the performance of the HPBW can be optimized [25]. It is worth mentioning that the 3-dB ARBW is exceedingly wide with compact size compare to the previous works. It shows that the proposed antenna is, to the best of our knowledge, the first of its type to achieve wide 3-dB ARBW of 241°.

IV. CONCLUSION

In this work, a CP antenna with wide 3-dB ARBW was firstly introduced. Its overall size is 60 × 60 mm^2, and it is fed by a 50-Ω coaxial feed. By studying the structure evolution, the CP characteristics were preliminarily analyzed. The antenna operates in RHCP radiation as illustrated by virtue of the surface current distribution on the patch, in which the two polarized degenerate modes TM10 and TM01 are generated to excite CP radiation. An equivalent circuit was utilized to

further study the working principle of the proposed antenna. Both the simulated and measured results show that the proposed antenna is promising for high elevation wireless application.

REFERENCES

[1] Y. Dong, S. Gao, Q. Luo, L. Wen, C.-X. Mao, S.-W. Dong, X. Li, G. Wei, G. Wen, Y. Geng, and Z. Cheng, "Broadband circularly polarized filtering antennas," *IEEE Access*, vol. 6, pp. 76302–76312, 2018.

[2] Z. Liu, Y. Zhang, Y. He, and Y. Li, "A compact-size and high-efficiency cage antenna for 2.4-GHz WLAN access points," *IEEE Trans. Antennas Propag.*, vol. 70, no. 12, pp. 12317–12321, Dec. 2022.

[3] M. Nosrati and N. Tavassolian, "Miniaturized circularly polarized square slot antenna with enhanced axial-ratio bandwidth using an antipodal Y-strip," *IEEE Antennas Wireless Propag. Lett.*, vol. 16, pp. 817–820, 2017.

[4] Y. Nasimuddin, S. Anjani, and A. Alphones, "A wide-beam circularly polarized asymmetric-microstrip antenna," *IEEE Trans. Antennas Propag.*, vol. 63, no. 8, pp. 3764–3768, Aug. 2015.

[5] J.-M. Laheurte, "Dual-frequency circularly polarized antennas based on stacked monofilar square spirals," *IEEE Trans. Antennas Propag.*, vol. 51, no. 3, pp. 488–492, Mar. 2003.

[6] X. Bai, S.-W. Qu, S. Yang, J. Hu, and Z.-P. Nie, "Millimeter-wave circularly polarized tapered-elliptical cavity antenna with wide axial-ratio beamwidth," *IEEE Trans. Antennas Propag.*, vol. 64, no. 2, pp. 811–814, Feb. 2016.

[7] X. Chen, D. Wu, L. Yang, and G. Fu, "Compact circularly polarized microstrip antenna with cross-polarization suppression at low-elevation angle," *IEEE Antennas Wireless Propag. Lett.*, vol. 16, pp. 258–261, 2017.

[8] Y. Luo, Q.-X. Chu, and L. Zhu, "A miniaturized wide-beamwidth circularly polarized planar antenna via two pairs of folded dipoles in a square contour," *IEEE Trans. Antennas Propag.*, vol. 63, no. 8, pp. 3753–3759, Aug. 2015.

[9] Y.-X. Sun, K. W. Leung, and K. Lu, "Broadbeam cross-dipole antenna for GPS applications," *IEEE Trans. Antennas Propag.*, vol. 65, no. 10, pp. 5605–5610, Oct. 2017.

[10] Y.-X. Sun, K. W. Leung, and J. Ren, "Dual-band circularly polarized antenna with wide axial ratio beamwidths for upper hemispherical coverage," *IEEE Access*, vol. 6, pp. 58132–58138, 2018.

[11] B.-C. Park and J.-H. Lee, "Compact circularly polarized antenna with wide 3-dB axial-ratio beamwidth," *IEEE Antennas Wireless Propag. Lett.*, vol. 15, pp. 410–413, 2016.

[12] M. K. Ray, K. Mandal, and N. Nasimuddin, "Low-profile circularly polarized patch antenna with wide 3 dB beamwidth," *IEEE Antennas Wireless Propag. Lett.*, vol. 18, no. 12, pp. 2473–2477, Dec. 2019.

[13] B. Yuan, X. H. Zhang, Z. F. Hu, and G. Q. Luo, "An axial-ratio beamwidth enhancement of patch antenna with digonal slot and square ring," *Microw. Opt. Technol. Lett.*, vol. 58, no. 3, pp. 672–675, Mar. 2016.

[14] M.-S. Wang, X.-Q. Zhu, Y.-X. Guo, and W. Wu, "Compact circularly polarized patch antenna with wide axial-ratio beamwidth," *IEEE Antennas Wireless Propag. Lett.*, vol. 17, no. 4, pp. 714–718, Apr. 2018.

[15] H. B. Wang, Y. J. Cheng, and Z. N. Chen, "Dual-band miniaturized linear-to-circular metasurface polarization converter with wideband and wide-angle axial ratio," *IEEE Trans. Antennas Propag.*, vol. 69, no. 12, pp. 9021–9025, Dec. 2021.

[16] S. B. Vignesh, Nasimuddin, and A. Alphones, "Stubs-integrated-microstrip antenna design for wide coverage of circularly polarised radiation," *IET Microw., Antennas Propag.*, vol. 11, no. 4, pp. 444–449, Mar. 2017.

[17] D. Schaubert, F. Farrar, A. Sindoris, and S. Hayes, "Microstrip antennas with frequency agility and polarization diversity," *IEEE Trans. Antennas Propag.*, vol. AP-29, no. 1, pp. 118–123, Jan. 1981.

[18] M. K. Ray, K. Mandal, N. Nasimuddin, A. Lalbakhsh, R. Raad, and F. Tubbal, "Two-pair slots inserted CP patch antenna for wide axial ratio beamwidth," *IEEE Access*, vol. 8, pp. 223316–223324, 2020.

[19] K. Itoh and T. Adachi, "Novel circularly polarized antennas combining a slot with parasitic dipoles," in *Proc. Antennas Propag. Soc. Int. Symp.*, Jun. 1980, pp. 52–55.

[20] Y. Liu, X. Li, L. Yang, and Y. Liu, "A dual-polarized dual-band antenna with omni-directional radiation patterns," *IEEE Trans. Antennas Propag.*, vol. 65, no. 8, pp. 4259–4262, Aug. 2017.

[21] M. I. Aksun, S.-L. Chuang, and Y. T. Lo, "On slot-coupled microstrip antennas and their applications to CP operation-theory and experiment," *IEEE Trans. Antennas Propag.*, vol. 38, no. 8, pp. 1224–1230, Aug. 1990.

[22] Z. Zhao, F. Liu, J. Ren, Y. Liu, and Y. Yin, "Dual-sense circularly polarized antenna with a dual-coupled line," *IEEE Antennas Wireless Propag. Lett.*, vol. 19, no. 8, pp. 1415–1419, Aug. 2020.

[23] X. Zhang, L. Zhu, and N.-W. Liu, "Pin-loaded circularly-polarized patch antennas with wide 3-dB axial ratio beamwidth," *IEEE Trans. Antennas Propag.*, vol. 65, no. 2, pp. 521–528, Feb. 2017.

[24] K.-B. Ng, C. H. Chan, and K.-M. Luk, "Low-cost vertical patch antenna with wide axial-ratio beamwidth for handheld satellite communications terminals," *IEEE Trans. Antennas Propag.*, vol. 63, no. 4, pp. 1417–1424, Apr. 2015.

[25] J.-H. Ou, S.-W. Dong, J. Huang, X. Y. Zhang, W. Che, and Q. Xue, "A compact microstrip antenna with extended half-power beamwidth and harmonic suppression," *IEEE Trans. Antennas Propag.*, vol. 68, no. 6, pp. 4312–4319, Jun. 2020.

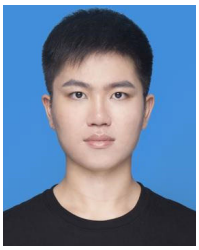

BO-WEN ZHENG received the B.E. degree from Hangzhou Dianzi University, Hangzhou, China, in 2021, where he is currently pursuing the M.E. degree, with a focus on wide beamwidth circularly polarized microstrip antenna.

BO YUAN received the B.E. and Ph.D. degrees from Wuhan University, Wuhan, China, in 2005 and 2012, respectively. He is currently a Faculty Member with Hangzhou Dianzi University, Hangzhou, China. His current research interest includes the design and applications of microwave components.

PENG ZHAO (Member, IEEE) received the B.E. and M.Phil. degrees from Zhejiang University, Hangzhou, China, in 2006 and 2008, respectively, and the Ph.D. degree from the City University of Hong Kong, in 2014. He is currently a Faculty Member with Hangzhou Dianzi University, Hangzhou. His current research interests include computational electromagnetics and antennas.

GAO-FENG WANG (Senior Member, IEEE) received the Ph.D. degree in electrical engineering from the University of Wisconsin–Milwaukee, WI, USA, in 1993, and the Ph.D. degree in scientific computing from Stanford University, CA, USA, in 2001. He is currently a Distinguished Professor with Hangzhou Dianzi University, Hangzhou, China. His current research interests include computational electromagnetics, electronic design automation, and antennas.